JACS
JOURNAL OF THE AMERICAN CHEMICAL SOCIETY
Communication
pubs.acs.org/JACS

Hollow Carbon-Nanotube/Carbon-Nanofiber Hybrid Anodes for Li-Ion Batteries

Yuming Chen,[†,∥,⊥] Xiaoyan Li,[†,⊥] Kyusung Park,[∥] Jie Song,[∥] Jianhe Hong,[∥] Limin Zhou,*[,†] Yiu-Wing Mai,[†,§] Haitao Huang,[‡] and John B. Goodenough*[,∥]

[†]Department of Mechanical Engineering and [‡]Department of Applied Physics, The Hong Kong Polytechnic University, Hong Kong, China

[§]Centre for Advanced Materials Technology (CAMT), School of Aerospace, Mechanical and Mechatronics Engineering J07, The University of Sydney, NSW 2006, Australia

[∥]Texas Materials Institute and Materials Science and Engineering Program, The University of Texas at Austin, Austin, Texas 78712, United States

Supporting Information

ABSTRACT: By a novel *in situ* chemical vapor deposition, activated N-doped hollow carbon-nanotube/carbon-nanofiber composites are prepared having a superhigh specific Brunauer–Emmett–Teller (BET) surface area of 1840 $m^2\ g^{-1}$ and a total pore volume of 1.21 $m^3\ g^{-1}$. As an anode, this material has a reversible capacity of ~1150 mAh g^{-1} at 0.1 A g^{-1} (0.27 C) after 70 cycles. At 8 A g^{-1} (21.5 C), a capacity of ~320 mAh g^{-1} fades less than 20% after 3500 cycles, which makes it a superior anode material for a Li-ion battery .

There has been an increasing demand for long-term and high-performance rechargeable lithium-ion batteries (LIBs) for a wide range of applications ranging from consumer devices and portable electronics to electric vehicles, hybrid electric vehicles, and large-scale grid energy storage.[1−4] Unfortunately, the energy density and power capability of graphite that is the current commercial anode material remains insufficient for next-generation LIBs.[5,6] Over the years, development and research efforts have been made to address these problems, including decreasing the material size,[7] designing one-dimensional (1D) nanostructured carbon including carbon nanotubes (CNTs) and carbon nanofibers (CNFs),[8,9] creating porous, hollow, and defect structures,[10−12] doping other elements such as boron and nitrogen,[13,14] and increasing the degree of graphitization.[11] Therefore, various nanostructured carbonaceous materials with high energy density or power capability have been successfully prepared. However, insufficient emphasis has been placed on solving the durability of electrodes with high energy density and power capability. Recently, significant progress has been made in combining these advantages (for example: 1D porous CNTs or CNFs,[15,16] 1D N-doped nanostructures,[17] N-doped graphene,[13] and nanoscaled hybrid materials[18]) to develop new high-performance and long-lasting carbon anodes. But it can be difficult to control and produce a good combination of pore size, pore number, N-doping, and a high degree of graphitization. Therefore, exploring and developing a novel approach to the synthesis of controlled 1D N-doped porous graphitic carbon nanomaterials for high-performance and long-term LIBs is urgently required.

In this communication, we design a novel *in situ* chemical vapor deposition to grow CNTs on the surface of N-doped CNFs by calcining a polymer to produce C_2H_2 that serves as a carbon source under the effect of Ni nanoparticles, yielding the activated N-doped hollow CNT-CNF hybrid materials with a superhigh specific Brunauer–Emmett–Teller (BET) surface area of 1840 $m^2\ g^{-1}$and a total pore volume of 1.21 $m^3\ g^{-1}$. In the resulting structure, the CNTs occupy the space between the CNFs while retaining access on all sides to the electrolyte. Compared to that of ref 11, this architecture enhances the density of actived material and improves remarkablely the anode volumetric capacity at high rates of charge/discharge. The inside and outside diameters of the CNTs grown on the surface of porous CNFs with attached hollow spheres are ~20 and 30 nm, respectively. The walls of the hollow carbon nanospheres and CNTs contain many defects. The prepared novel material has a doping level of ~1.4 wt % nitrogen and, as an anode, shows an exceptional reversible capacity of ~1530 mAh g^{-1} at 0.1 A g^{-1}, outstanding rate capability, and long cycling stability of over 3500 times while retaining more than 80% capacity at 8 A g^{-1}.

Polyacrylonitrile/nickel acetate/poly(methyl methacrylate) (PAN/$Ni(Ac)_2$/PMMA) composite nanofibers were first prepared by coaxial electrospinning. The as-collected nanofibers were stabilized at 250 °C for 2 h and then pyrolyzed at 700 °C in H_2/N_2 (5%/95%) for 6 h. The PMMA was completely decomposed to produce pores and C_2H_2 that served as a carbon source for the growth of CNTs under the effect of Ni nanoparticles formed by the decomposition of $Ni(Ac)_2$.[19−24] The PAN with a high N content (~26.4 wt %) on the surface of the Ni nanoparticles was carbonized into N-doped graphitic carbon under the catalytic effect of Ni.[12] As shown in Figure 1a, N-doped CNT–CNF–Ni hybrid materials were fabricated. Finally, activated N-doped hollow CNT–CNF hybrid materials were prepared by a combination of KOH activation and HNO_3

Received: August 14, 2013
Published: October 21, 2013

 © 2013 American Chemical Society dx.doi.org/10.1021/ja408421n | J. Am. Chem. Soc. 2013, 135, 16280−16283

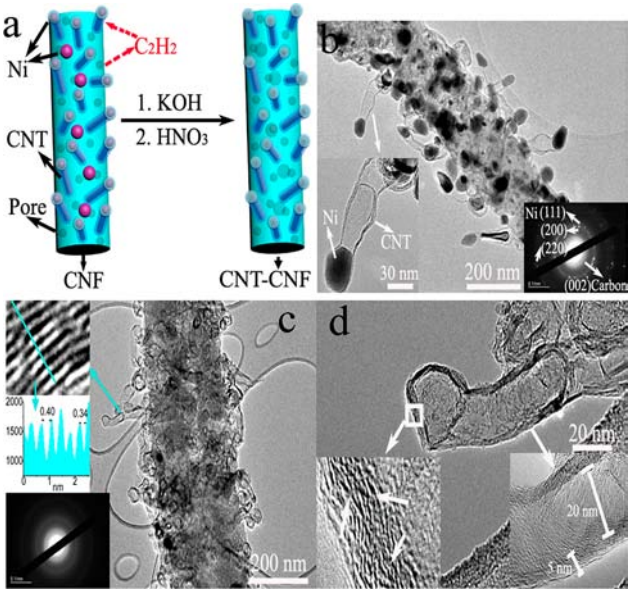

Figure 1. (a) Schematic of the activated N-doped hollow CNT−CNF hybrid material design. The PMMA was decomposed to produce pores and C_2H_2 that served as a carbon source for the growth of CNTs on the surface of CNFs under the effect of Ni nanoparticles. (b) SAED pattern and TEM image of the N-doped CNT−CNF−Ni hybrid material. (c) SAED pattern and TEM image of the activated N-doped hollow CNT−CNF hybrid material, and line profiles of the *d*-spacing of graphene sheets of the wall of CNT. (d) TEM and HRTEM images of CNT, revealing the presence of defects in the wall of hollow structure.

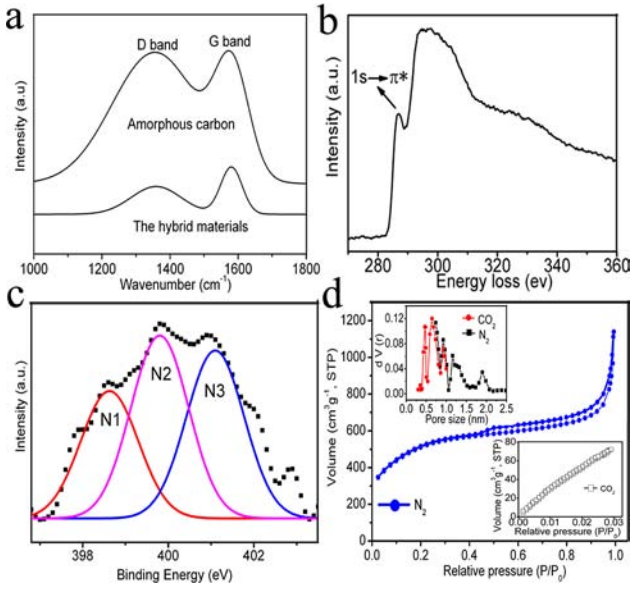

Figure 2. (a) Raman spectra of amorphous carbon and the activated N-doped hollow CNT−CNF hybrid materials. (b) EELS spectra of the activated N-doped hollow CNT−CNF hybrid material. (c) N1 XPS spectra of the activated N-doped hollow CNT−CNF hybrid material. Three components represent pyridinic (N1, ∼398.6 eV), pyrrolic (N2, 400.1 eV), and graphitic (N3, ∼401.4 eV) N atoms, respectively. (d) Nitrogen and CO_2 adsorption−desorption isotherms and pore-size distributions (inset) of the activated N-doped hollow CNT-CNF hybrid material.

treatment to remove the Ni and achieve high BET surface area with high total pore volume.

Transmission electron microscopy (TEM, Figure 1b) and high-resolution TEM (HRTEM, Figure S-1a) images show that the multiwalled CNTs formed from Ni/carbon composite nanofibers and the Ni nanoparticles were encapsulated in graphitic carbon with a thickness of ∼5 nm as compared with CNFs and Ni/carbon nanofibers (Figure S-2). The interplanar spacing of ∼0.23 nm corresponds to the (010) plane of Ni. The spot- and ring-like patterns in the selected area electron diffraction (SAED,inset of Figure 1b) and X-ray diffraction pattern (XRD, Figure S-3) further confirm the presence of crystalline Ni and carbon. The low- and high-magnification TEM images in Figure 1c,d show that the inside and outside diameters of CNTs are ∼20 and 30 nm, respectively. Figure S-1b,c shows that the CNFs possess many pores and hollow carbon nanoparticles. Line profiles exhibit that the *d*-spacing of the graphene sheets in the CNFs and CNTs, which is due to the (002) plane of carbon, is in the range of 0.34−0.42 nm (Figure 1c inset, and Figure S-1e). The SAED pattern displays (Figure 1c, inset) ring-like patterns, suggesting that the synthesized hybrid material is graphitic. Additionally, HRTEM images (Figure 1d inset and Figure S-1d) show that the wall of the hollow structure consists of many defects between discontinuous graphene sheets as indicated by the arrows.

Raman-spectrum analyses in Figure 2a indicate that the G-band of the activated hybrid materials has a greatly enhanced intensity. The ratio ($R = I_G/I_D$) of the intensity of the G-band to the intensity of the D-band is ∼1.46, which is higher than that of amorphous CNFs (∼0.95), indicating a great increase in the degree of graphitic crystalline structure because of the use of Ni nanoparticles as a catalyst for promoting the graphitization of carbon. The electron energy loss spectrum (EELS) of the prepared materials in Figure 2b shows a prepeak of carbon located at ∼258 eV corresponding to the transitions to π^* states in the sp^2 carbon, which confirms the existence of graphene sheets in the activated N-doped hollow CNT−CNF hybrid materials.[25] A doping level of ∼1.4 wt % nitrogen in the activated hollow hybrid carbon was determined by element analysis. In the XPS N1s spectrum of the obtained carbon shown in Figure 2c, three components represent pyridinic (N1, ∼398.6 eV), pyrrolic (N2, 400.1 eV), and graphitic (N3, ∼401.4 eV) N atoms, respectively.[13] The N binding configuration includes 26.6% pyridinic N, 38.0% pyrrolic N, and 35.4% graphitic N. XPS C1s spectra were also obtained, and similar conclusions were reached (Figure S-4). The specific BET surface area of the activated hybrid carbon is 1840 $m^2\ g^{-1}$ with a total pore volume of 1.21 $m^3\ g^{-1}$, which is much higher than that of hybrid carbon (371 $m^2\ g^{-1}$). Figure 2d shows the nitrogen adsorption−desorption isotherms of the activated hollow hybrid materials. The strong nitrogen adsorption below the relative to atmospheric pressure of 0.1 is characteristic of micropore filling. The continuous rise of adsorption−desorption isotherms in the relative pressure range from 0.1 to 1 indicates the presence of mesopore (0.1−0.6) and macropores (0.6−1) in the resultant materials.[26] Figure 2d (inset) displays the results of a pore size analysis by applying a hybrid nonlocal density functional theory (NLDFT). It is evident that the activated hybrid materials possess many micropores peaked at ∼0.35, 0.48, 0.64, 0.9, 1.1, 1.3, and 1.9 nm, respectively. A broad peak from 3 to 151 nm can also be observed (Figure S-5). These findings are due to the defect, porous structure and hollow structure in the obtained carbon.

dx.doi.org/10.1021/ja408421n | J. Am. Chem. Soc. 2013, 135, 16280−16283

These results are consistent with the TEM and HRTEM observations.

Figure 3a shows the galvanostatic charge−discharge profiles of the activated N-doped hollow CNT−CNF hybrid materials

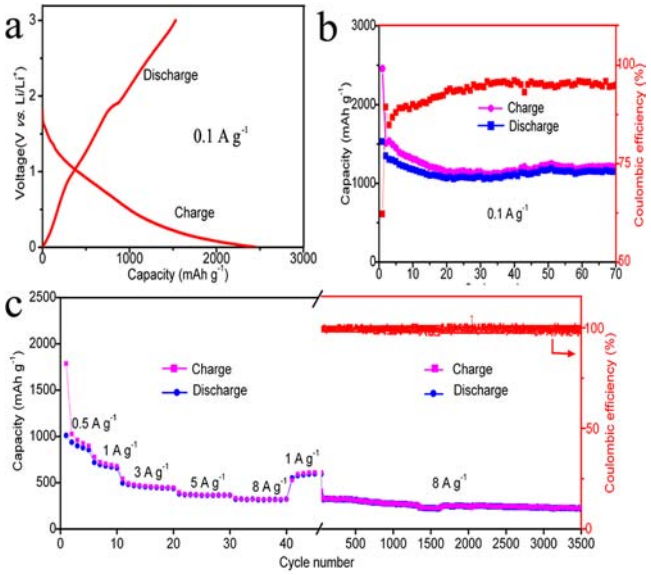

Figure 3. (a−c) Charge−discharge voltage profiles, capacities at various rates, and cycling performances of the activated N-doped hollow CNT−CNF hybrid electrodes tested between 3 and 0 V versus Li^+/Li.

at 0.1 A g^{-1} in the voltage range 0−3 V versus Li^+/Li. During the first cycle, the voltage plateau at ∼0.7 V is ascribed to the formation of a solid electrolyte interface (SEI) layer and electrolyte decomposition.[27] The first charge and discharge specific capacities are ∼2458 and 1530 mAh g^{-1}. The large irreversible capacity can be attributed to SEI formation.[17,28] In addition, the prepared materials also show remarkable high-power rate capability. At current densities of 0.5, 1, 3, 5, and 8 A g^{-1}, the reversible capacities of the activated hollow hybrid materials are ∼940, 700, 500, 380, and 320 mAh g^{-1}, respectively (Figure 3c). Figure S-6 shows a typical cyclic voltammogram of the activated N-doped hollow CNT−CNF hybrid electrode. There are two reduction peaks of ∼1.3 and 0.7 V in the first cycle that are ascribed to the irreversible reactions between the activated hollow hybrid carbon electrode and electrolyte and the cointercalation of solvated lithium ions into graphene sheets.[11,12] During the third cycle to the fifth cycle, there is no clear change, suggesting that the activated hollow hybrid carbon electrode is stable with reversible reactions during the following charge−discharge cycles. The cycling performance of the activated N-doped hollow CNT−CNF hybrid electrodes is present in Figure 3b,c. The capacity of synthesized materials becomes stable and reversible after the initial few cycles. The Coulombic efficiencies of the activated hollow hybrid materials at both low and high current density remain more than ∼95% after the initial few cycles. The capacity remains ∼1150 mAh g^{-1} at 0.1 A g^{-1} (0.27 C) after 70 cycles and has a fading of less than 20% at 8 A g^{-1} (21.5 C) after 3500 cycles. Moreover, the volumetric capacity of the synthesized hybrid electrode can be up to ∼1.7 Ah cm^{-3} at 0.1 A g^{-1}, which is ∼2.0 times higher than that of graphite (∼0.84 Ah cm^{-3}). This performance is superior to that of other carbon materials, metal oxide, metal, and hybrid materials.[10,29−33] Additionally, this material still has high capacities of ∼913, 606, 381, 268, 214, and 181 mAh g^{-1} at current densities of 0.1, 0.5, 1, 3, 5, and 8 A g^{-1}, respectively, tested between 2 and 0 V versus Li^+/Li (Figure S7). The low Coulombic efficiency observed for the hybrid in the first cylce (Figure 3a and Figure S7a) can be improved by introducing closed pores that only allow the access of Li^+ without the electrolyte, and forming a passivation layer on the surface of the anode.[6]

The remarkable electrochemical performance of the activated N-doped hollow CNT−CNF hybrid materials is the result of their novel structure, N-doping, 1D nanostructure, and high electrical conductivity of 20.2 S cm^{-1}.[31] Many defects in the obtained materials, large numbers of pores and hollow spheres, and the large *d*-spacing of graphene sheets would serve as reservoirs for the storage of Li^+.[16−18] CNTs on the surface of CNFs are favorable for lithium-ion diffusion from different directions and provide sufficient contact between active material and electrolyte for absorbing Li ions and increasing the rapid charge-transfer reaction.[5] The porous structure and high specific surface area can reduce the diffusion length of Li ions. On the other hand, many defects in the hybrid materials can allow the diffusion of Li^+ from outside carbon into the inner carbon, which activates all the carbon material. Additionally, N-doping in the hybrid materials can enhance the electrochemical reactivity and electronic conductivity, which further promotes the excellent electrochemical performance.[17]

In summary, we have developed a novel *in situ* chemical vapor deposition for preparing activated N-doped hollow CNT−CNF hybrid materials with a superhigh specific surface area of 1840 m^2 g^{-1}. The prepared hybrid materials as anode electrodes showed excellent electrochemical performance with a good combination of a high reversible specific capacity and a remarkable volumetric capacity, outstanding rate capability, and long cycling stability. The novel method can be extended to obtain various porous carbon−CNT hybrid materials for applications in sensors, electronic and electrochemical devices, catalysts, and hydrogen storage materials.

■ ASSOCIATED CONTENT

Supporting Information

Detailed experimental methods, TEM, HRTEM, XRD, XPS, and electrochemical characterization. This material is available free of charge via the Internet at http://pubs.acs.org.

■ AUTHOR INFORMATION

Corresponding Authors

mmlmzhou@polyu.edu.hk
jgoodenough@mail.utexas.edu

Author Contributions

⊥These authors contributed equally.

Notes

The authors declare no competing financial interest.

■ ACKNOWLEDGMENTS

The authors are grateful for the support received from the Research Grants Council of the Hong Kong Special Administration Region (grants: PolyU 5349/10E and PolyU 5312/12E) and the Hong Kong Polytechnic University (grants: G-YK47 and1-BD08). J.B.G. thanks the Robert A. Welch Foundation of Houston, TX (Grant F-1066).

REFERENCES

(1) Armand, M.; Tarascon, J. -M. *Nature* **2008**, *451*, 652−657.
(2) Kang, K.; Meng, Y. S.; Bréger, J.; Grey, C. P.; Ceder, G. *Science* **2006**, *311*, 977−980.
(3) Liu, N.; Wu, H.; McDowell, M. T.; Yao, Y.; Wang, C.; Cui, Y. *Nano Lett.* **2012**, *12*, 3315−3321.
(4) Goodenough, J. B.; Park, K. S. *J. Am. Chem. Soc.* **2013**, *135*, 1167−1176.
(5) Hu, Y. S.; Adelhelm, P.; Smarsly, B. M.; Hore, S.; Antonietti, M.; Maier, J. *Adv. Funct. Mater.* **2007**, *17*, 1873−1878.
(6) Kaskhedikar, N. A.; Maier, J. *Adv. Mater.* **2009**, *21*, 2664−2680.
(7) Deng, D.; Lee, J. Y. *Chem. Mater.* **2007**, *19*, 4198−4204.
(8) Claye, A. S.; Fischer, J. E.; Huffman, C. B.; Rinzler, A. G.; Smalley, R. E. *J. Electrochem. Soc.* **2000**, *147*, 2845−2852.
(9) Shen, J. M.; Feng, Y. T. *J. Phys. Chem. C* **2008**, *112*, 13114−13120.
(10) Fang, Y.; Lv, Y. Y.; Che, R. C.; Wu, H. Y.; Zhang, X. H.; Gu, D.; Zheng, G. F.; Zhao, D. Y. *J. Am. Chem. Soc.* **2013**, *135*, 1524−1530.
(11) Chen, Y. M.; Lu, Z. G.; Zhou, L. M.; Mai, Y. W.; Huang, H. T. *Nanoscale* **2012**, *4*, 6800−6805.
(12) Chen, Y. M.; Lu, Z. G.; Zhou, L. M.; Mai, Y. W.; Huang, H. T. *Energy Environ. Sci.* **2012**, *5*, 7898−7902.
(13) Wu, Z. S.; Ren, W. C.; Xu, L.; Li, F.; Cheng, H. M. *ACS Nano* **2011**, *5*, 5463−5471.
(14) Shin, W. H.; Jeong, H. M.; Kim, B. G.; Kang, J. K.; Choi, J. W. *Nano Lett.* **2012**, *12*, 2283−2288.
(15) Ji, L. W.; Zhang, X. W. *Electrochem. Commun.* **2009**, *11*, 684−687.
(16) Ji, L. W.; Zhang, X. W. *Nanotechnology* **2009**, *20*, 155705−1557011.
(17) Qie, L.; Chen, W. M.; Wang, Z. H.; Shao, Q. G.; Li, X.; Yuan, L. X.; Hu, X. L.; Zhang, W. X.; Huang, Y. H. *Adv. Mater.* **2012**, *24*, 2047−2050.
(18) Fan, Z. J.; Yan, J.; Wei, T.; Ning, G. Q.; Zhi, L. J.; Liu, J. C.; Cao, D. X.; Wang, G. L.; Wei, F. *ACS Nano* **2011**, *5*, 2787−2794.
(19) Burge, S. J.; Tipper, C. F. H. *Combust. Flame* **1969**, *13*, 495−505.
(20) Kashiwagi, T.; Inaba, A.; Brown, J. E.; Hatada, K.; Kitayama, T.; Masuda, E. *Macromolecules* **1986**, *19*, 2160−2168.
(21) Manring, L. E. *Macromolecules* **1988**, *21*, 528−530.
(22) Lin, M.; Tan, J. P. Y.; Boothroyd, C.; Loh, K. P.; Tok, E. S.; Foo, Y. L. *Nano Lett.* **2006**, *6*, 449−452.
(23) Helveg, S.; Lopez-Cortes, C.; Sehested, J.; Hansen, P. L.; Clausen, B. S.; Rostrup-Nielsen, J. R.; Abild-Pedersen, F.; Nørskov, J. K. *Nature* **2004**, *427*, 426−429.
(24) Li, X. S.; Cao, A. Y.; Jung, Y. J.; Vajtai, R.; Ajayan, P. M. *Nano Lett.* **2005**, *5*, 1997−2000.
(25) Schlittler, R. R.; Seo, J. W.; Gimzewski, J. K.; Durkan, C.; Saifullah, M. S. M.; Welland, M. E. *Science* **2001**, *292*, 1136−1139.
(26) Zhang, L. L.; Zhao, X.; Stoller, M. D.; Zhu, Y. W.; Ji, H. X.; Murali, S.; Wu, Y. P.; Perales, S.; Clevenger, B.; Ruoff, R. S. *Nano Lett.* **2012**, *12*, 1806−1812.
(27) Bulusheva, L. G.; Okotrub, A. V.; Kurenya, A. G.; Zhang, H.; Zhang, H.; Chen, X.; Song, H. *Carbon* **2011**, *49*, 4013−4023.
(28) Zhang, B.; Zheng, Q. B.; Huang, Z. D.; Oh, S. W.; Kim, J. K. *Carbon* **2011**, *49*, 4524−4534.
(29) Reddy, A. L. M.; Srivastava, A.; Gowda, S. R.; Gullapalli, H.; Dubey, M.; Ajayan, P. M. *ACS Nano* **2010**, *4*, 6337−6342.
(30) Wang, C.; Zhou, Y.; Ge, M. Y.; Xu, X. B.; Zhang, Z. L.; Jiang, J. Z. *J. Am. Chem. Soc.* **2010**, *132*, 46−47.
(31) Wang, H. L.; Cui, L. F.; Yang, Y.; Casalongue, H. S.; Robinson, J. T.; Liang, Y. Y.; Cui, Y.; Dai, H. J. *J. Am. Chem. Soc.* **2010**, *132*, 13978−13980.
(32) Reddy, A. L. M.; Shaijumon, M. M.; Gowda, S. R.; Ajayan, P. M. *Nano Lett.* **2009**, *9*, 1002−1006.
(33) Yu, Y.; Gu, L.; Zhu, C. B.; van Aken, P. A.; Maier, J. *J. Am. Chem. Soc.* **2009**, *131*, 15984−15985.